batteries

Article

Synchronously Stabilizing the Interphase of Cathode and Anode Enabling Lithium Metal Batteries via Multiple Electrolyte Additives

Yi Wan [1], Weihang Bai [1], Shun Wu [1], Che Sun [1], Shuaishuai Chen [1], Yinping Qin [1,*], Muqin Wang [2,*], Zhenlian Chen [1], Mingkui Wang [2] and Deyu Wang [1,*]

[1] Key Laboratory of Optoelectronic Chemical Materials and Devices, The Ministry of Education, School of Optoelectronic Materials & Technology, Jianghan University, Wuhan 430056, China; wanyi@stu.jhun.edu.cn (Y.W.); 2411608872@stu.jhun.edu.cn (W.B.); liushisan13@foxmail.com (S.W.); sunche1236697@stu.jhun.edu.cn (C.S.); youcaivp@mail.ustc.edu.cn (S.C.); zhenlianchen@jhun.edu.cn (Z.C.)
[2] Wuhan National Laboratory for Optoelectronics, Huazhong University of Science and Technology, Wuhan 430074, China; mingkui.wang@hust.edu.cn
* Correspondence: clqinyinping@126.com (Y.Q.); mokinwong@163.com (M.W.); wangdeyu@jhun.edu.cn (D.W.)

Abstract: As the most promising high energy density technology, lithium metal batteries are associated with serious interfacial challenges because the electrolytes employed are unable to meet the requirements of both electrodes simultaneously, namely, the systems that work for Li metal are highly likely to be unsuitable for the cathode, and vice versa. In this study, we investigate the synergistic effects of lithium bis (oxalate) borate (LiBOB), fluoroethylene carbonate (FEC) and adiponitrile (ADN) to develop a formula that is compatible with both elements in the battery. The solid–electrolyte interphase (SEI) multi-layer generated from LiBOB and FEC successfully protects the electrolyte from the lithium and suppresses the decomposition of ADN on lithium, identified by the tiny amounts of isonitriles on the surface of the anode. Simultaneously, most of the ADN molecules remain and protect the cathode particles via the absorption layer of the nitrile groups, in the same way that this process works in commercial lithium-ion batteries. Benefiting from the stable interfacial films formed synchronously on the anode and cathode, the $Li/LiNi_{0.8}Co_{0.1}Mn_{0.1}O_2$ cells with an area capacity of ~3 mAh cm^{-2} operate stably beyond 250 cycles and target the accumulated capacity to levels as high as ~653.4 mAh cm^{-2}. Our approach demonstrates that electrolyte engineering with known additives is a practical strategy for addressing the challenges of lithium batteries.

Keywords: electrolyte additives; forming SEI and CEI synchronously; Li metal batteries

Citation: Wan, Y.; Bai, W.; Wu, S.; Sun, C.; Chen, S.; Qin, Y.; Wang, M.; Chen, Z.; Wang, M.; Wang, D. Synchronously Stabilizing the Interphase of Cathode and Anode Enabling Lithium Metal Batteries via Multiple Electrolyte Additives. *Batteries* **2024**, *10*, 338. https://doi.org/10.3390/batteries10100338

Academic Editors: Yujing Bi, Yaocai Bai and Claudio Gerbaldi

Received: 26 August 2024
Revised: 12 September 2024
Accepted: 16 September 2024
Published: 24 September 2024

1. Introduction

With its highest specific capacity of 3860 mAh g^{-1} and its lowest reduction potential of −3.04 V vs. S.H.E., Li metal has been considered the ideal anode for energy storage devices [1,2]. When coupled with layer structural materials such as $LiCoO_2$ and $LiNi_{0.82}Co_{0.06}Mn_{0.12}O_2$, lithium metal batteries could deliver an energy density of ~450 Wh h^{-1}, much higher than the state-of-art lithium-ion batteries [3,4]. However, this system faces a serious challenge in relation to its interfacial stability since the appropriate electrolytes for Li metal are highly likely to be unsuitable for an oxide cathode and vice versa. The harmful interfacial reactions on the cathode or anode eventually cause a rapid decay in capacity and a significant deterioration in lifespan. Therefore, it is essential to develop one electrolyte that is capable of constructing stable protective layers on both electrodes [5,6].

Significant efforts have been expended attempting to construct this protective layer and have obtained remarkable achievements [7–9], in particular in relation to the strategies of electrolyte engineering, which is the in situ formatting of SEI and CEI films

during electrochemical processes via the adjustment of the solvents, lithium salts and additives [10,11]. Kim et al. employed lithium nitrate and lithium difluoro (bisoxalato) phosphate (LiDFBP) additives to form a Li_3N- and LiF-rich SEI layer on a Li anode and LiDFPB-derived CEI on a Ni-rich cathode, thereby attaining excellent cycling performances from the Li/Ni-rich batteries [1]. Li et al. designed a sulfonamide-based electrolyte to simultaneously stabilize the interphases of the $LiCoO_2$ and Li metal electrodes, enabling a high Coulombic efficiency ~99.84% for $LiCoO_2$/Li cells at the cut-off voltage of 4.6 V vs. Li/Li^+ [2]. Lei et al. have reported a multi-functional electrolyte additive to build a robust CEI layer enriched with LiF/Li_3N components and an inorganic-rich SEI layer, enhancing the cycle stability of the $Li/LiNi_{0.8}Co_{0.1}Mn_{0.1}O_2$ cells [3] This progress in electrolyte engineering has provided a good basis for developing the chemical systems of the lithium battery.

Nitriles are a widely used additive for stabilizing cathode particles with a cut-off voltage lower than 4.35 V vs. Li/Li^+ in commercial lithium-ion batteries [12–15]. However, their application in lithium metal batteries has been unsuccessful due to the high reactivity of solvents to lithium and the continuously broken and repaired SEI layer on the lithium [12]. A high-quality SEI layer may be able to suppress the decomposition of nitriles on an anode and enable their practical utilization in lithium metal batteries. In our previous work, a high-quality SEI film that comprised a B-rich bottom layer, a LiF-rich middle layer and a hydrocarbon top layer was formed via the combination of FEC and LiBOB additives; however, the high ratio of fluorine solvents tended to corrode the cathode and accelerate the capacity fading [15]. An SEI film generated from the combination of LiBOB and FEC could probably alleviate the decomposition of nitriles on the lithium anode, and the protection of nitriles could further alleviate the harmful effects of the high-ratio F-contained solvents. Therefore, the electrolyte system with FEC, LiBOB and dinitrile solvent may synchronously form SEI and CEI films on the anode and cathode.

In this study, we investigate the synergistic effects of FEC, LiBOB and adiponitrile (ADN) on the durability of $Li/LiNi_{0.8}Co_{0.1}Mn_{0.1}O_2$ cells. After 75 cycles, significant quantities of side-products, including isonitriles and Li_3N, were accumulated on the lithium anode in the electrolyte, where only ADN (Base + ADN) was added. In contrast, only a tiny number of isonitriles and lithium nitride were detectable on the anode side in the electrolyte with FEC and LiBOB (Base + FEC + LiBOB + ADN), indicating ADN's decomposition was significantly suppressed in this system. The lower consumption of ADN is beneficial for protecting the cathode particles via the coordinative interaction of the ADN additive with the transition metals, which results in significant durability. Their working mechanism is illustrated in Scheme 1.

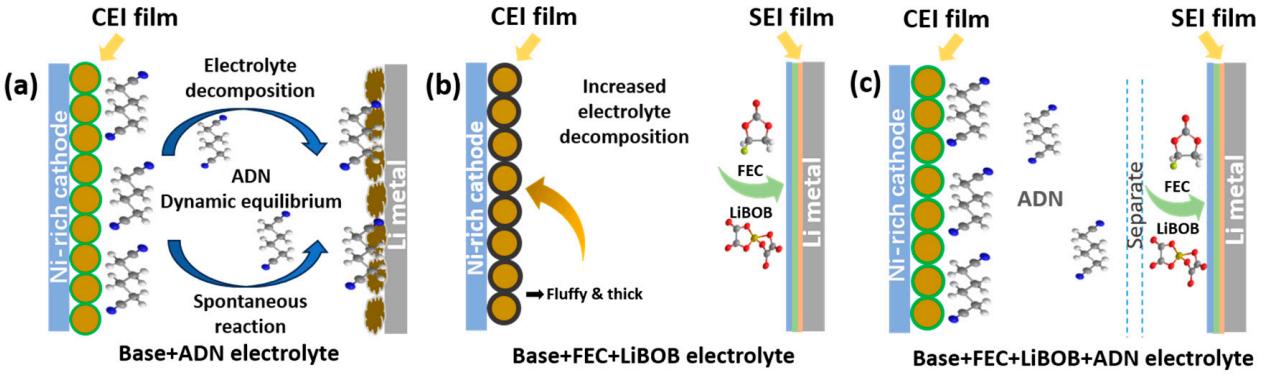

Scheme 1. The schematics of the electrode/electrolyte interphases in Base + ADN, Base + FEC + LiBOB and Base + FEC + LiBOB + ADN electrolytes. (**a**) Addition of ADN to the base electrolyte promotes the formation of a thin CEI on the cathode side, but ADN severely erodes the Li metal anode and produces a large number of by-products, and ADN is also consumed in large quantities at the cathode; (**b**) the addition of FEC and LiBOB can form a three-layer composite SEI to protect the

Li-metal anode, but the cathode side produces a fluffy and thick deposit; (**c**) when ADN and FEC and LiBOB are used simultaneously, a stable protective film can be formed on both sides, curbing the occurrence of the adverse reactions in (**a**,**b**).

2. Results and Discussion

Four types of electrolytes were investigated in this work. The 2 M of $LiPF_6$ dissolved in a mixture of ethylene carbonate (EC) and diethyl carbonate (DEC) (1:1, *v*/*v*) was denoted as the Base. To the other three electrolytes that comprised Base + ADN, Base + FEC + LiBOB and Base + FEC + LiBOB + ADN electrolytes, 1.0 wt.% ADN, 30.8 wt.% FEC and 1.2 wt.% LiBOB and 30.8 wt.% FEC, 1.2 wt.% LiBOB and 1.0 wt.% ADN were added to the Base electrolyte, respectively. As shown in Table S1, the ionic conductivity of the electrolytes without ADN is slightly lower than those with ADN but is still in the same order of magnitude, indicating the positive effect of the nitrile-based solvents on ionic transportation.

To investigate their behavior on anodes, the Li/Super-P cells were assembled with four electrolytes, and cyclic voltammogram (CV) tests were conducted. As shown in Figure 1a, in the first cycle, a strong peak at ~0.7 V vs. Li/Li^+ is observed in the Base electrolyte, corresponding to the reduction of the EC solvent according to previous reports [16]. The reductive peak of EC shifts to ~0.5 V vs. Li/Li^+ in the Base + ADN electrolyte, indicating that a significant polarization occurs on the Li anode, which is related to the thermodynamic reactions of the ADN with the Li metal. In the Base + FEC + LiBOB and Base + FEC + LiBOB + ADN electrolytes, there are two obvious peaks at 1.80 and 1.64 V vs. Li/Li^+, which are identified as being related to the reduction of the LiBOB and FEC additives, as shown in the results illustrated in Figure S2, and the reductive peak of EC is indistinct in both electrolytes. These results indicate that the film obtained from FEC and LiBOB on lithium prevents the thermodynamic or electrochemical decomposition of the carbonate-based solvents. Moreover, the reductive peaks of the FEC and LiBOB additives disappeared in the second cycle, indicating their significant efficiency in forming films (Figure 1b).

The oxidative stability of the four electrolytes is evaluated in the Li/Super-P cells, with a linear sweep voltammetry (LSV) measurement between 2.8 and 5.0 V vs. Li/Li^+. As shown in Figure 1c, the violent oxidation of the Base and the Base + FEC + LiBOB electrolytes occurs at ~4.3 V vs. Li/Li^+, while the Base + ADN and Base + FEC + LiBOB + ADN electrolytes can be positively pushed to 4.8 V and over 5.0 V vs. Li/Li^+. According to our previous work [17], the nitriles can be absorbed on a cathode forming an interfacial layer, isolating the electrolytes in direct contact with an aggressive cathode. However, most of the ADN in the Base + ADN electrolytes would be consumed on the anode because of the spontaneous reaction with the Li metal. Meanwhile, in the Base + FEC + LiBOB + ADN electrolyte, the film that has evolved from the FEC + LiBOB prevents the reaction; thereby, ADN plays a positive role in the interface of the cathode, improving the oxidative potential of the electrolyte.

To confirm the spontaneous reaction of ADN with Li metal and the effect of the FEC + LiBOB evolved film, the fresh and the cycled Li metals are soaked in an ADN solution; then, the surfaces' components are analyzed with an XPS measurement. As shown in Figure 1d,e, on the fresh Li metal and on that cycled in the Base electrolyte, two obvious peaks located at ~398.1 and 399.7 eV were identified, attributable to the Li_3N and -CN compounds. However, a weak peak located at ~399.8 eV was detected on the Li anode cycled in the Base + FEC + LiBOB + ADN electrolyte, without the appearance of Li_3N. These results demonstrate that the FEC and LiBOB additive-formed film can effectively prevent the reaction between the solvents and lithium metal. Therefore, the SEI film formed from suitable additives could suppress the decomposition of ADN, and most of the ADN molecules could remain and protect the cathode particles, as in commercial lithium-ion batteries.

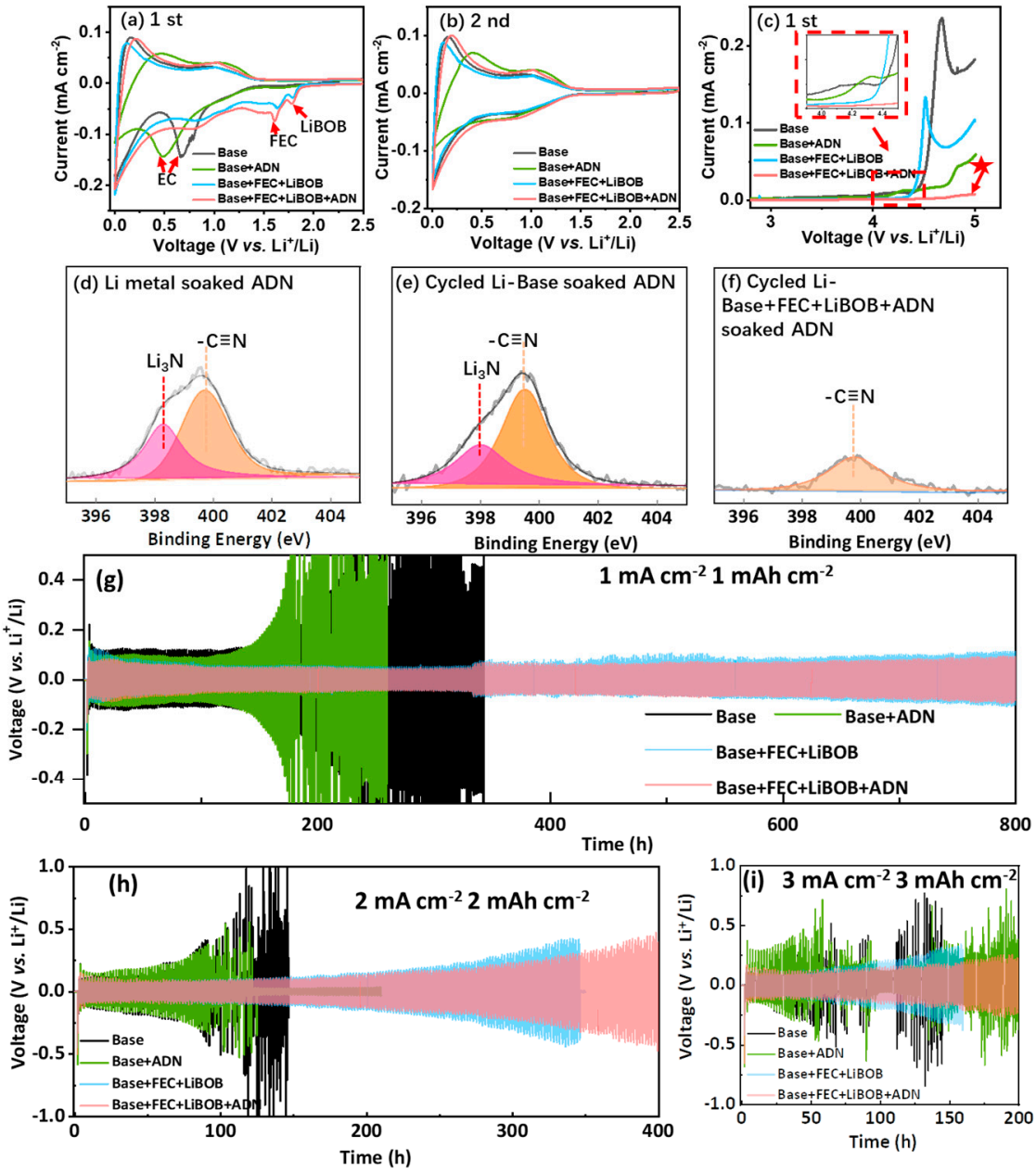

Figure 1. (**a**,**b**) The CV profiles of four electrolytes in Li/Super-P cells: (a) the first cycle; (**b**) the second cycle; (**c**) the LSV of four electrolytes in the Li/Super-P cells; (**d**–**f**) the N 1s spectrum of the Li anode soaked in an ADN solution by XPS: (**d**) fresh Li metal; (**e**) Li anode cycled in Base electrolyte; (**f**) Li anode cycled in Base + FEC + LiBOB + ADN electrolyte; (**g**–**i**) cyclic performances of the Li/Li symmetric cells in four electrolytes at different current densities and capacities: (**g**) 1 mA cm^{-2} and 1 mAh cm^{-2}; (**h**) 2 mA cm^{-2} and 2 mAh cm^{-2}; (**i**) 3 mA cm^{-2} and 3 mAh cm^{-2}.

To further verify the effect of the SEI film formed from FEC and LiBOB, the Li/Li symmetric cells were tested at different current densities. As shown in Figure 1g, at a plating current of 1 mA cm^{-2} and capacity of 1 mAh cm^{-2}, the cyclic performances of the symmetric cells are no more than 200 h with the Base and Base + ADN electrolytes. In sharp contrast, the Li metal electrodes with the FEC and LiBOB electrolytes show a stable cyclic performance over 800 h. At a plating current of 2 mA cm^{-2} and a capacity of 2 mAh cm^{-2}, the cells with the Base or Base + ADN electrolytes operate for no more than 100 h, while those with FEC- and LiBOB-added electrolytes operate for over 300 h. At a larger plating current of 3 mA cm^{-2} and a capacity of 3 mAh cm^{-2}, the cells with the Base and Base +

ADN electrolytes cannot work for more than 25 h; meanwhile, the cells with the Base + FEC + LiBOB electrolytes operate for over 150 h and those with the Base + FEC + LiBOB + ADN electrolytes operate for over 200 h. These results indicate that the FEC and LiBOB additives play a significant role in the stability of the Li anode, and the combination of multiple additives exhibits the best performance on the Li anode. In addition, the inclusion of ADN could slightly alleviate the polarization of the system.

The influence of the investigated electrolytes on the electrochemical properties was compared in the Li/$LiNi_{0.8}Co_{0.1}Mn_{0.1}O_2$ cells, as shown in Figure 2. The first discharge capacity rates (0.1C) are 182.4, 169.1, 185.6 and 192.3 mAh g^{-1} with a Coulombic efficiency of 87.97, 87.66, 88.02 and 90.23% for the cells with the Base electrolyte, Base + ADN, Base + FEC + LiBOB and Base + FEC + LiBOB + ADN, respectively, as shown in Table S2. The rate performances of the Li/$LiNi_{0.8}Co_{0.1}Mn_{0.1}O_2$ cells with four electrolytes were also tested. As shown in Figures 2h and S4, with the increase in the charging/discharging rate, the decrease in capacity in the Base and Base + ADN electrolytes is faster than that in the FEC- and LiBOB-added electrolytes. At 2 C, the discharge capacities of the cells in the Base, Base + ADN, Base + FEC + LiBOB and Base + FEC + LiBOB + ADN electrolytes are 14.5, 32.4, 104.2 and 113.2 mAh g^{-1}. This very significant difference should be attributed to the low interfacial impedances of the SEI films formed from FEC and LiBOB. Additionally, the ADN additive exerts a slight, positive effect on the discharge capacity.

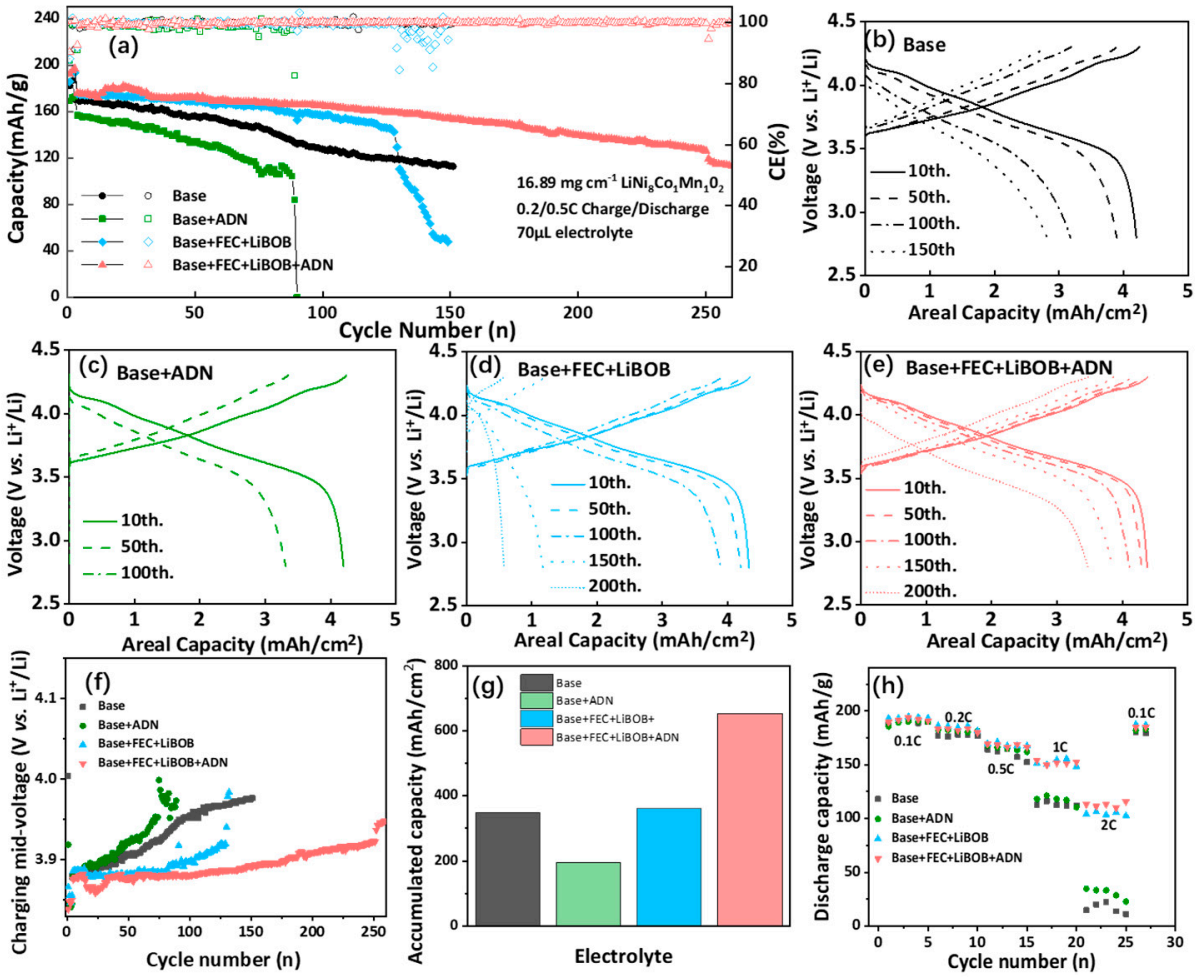

Figure 2. The electrochemical performances of Li/$LiNi_{0.8}Co_{0.1}Mn_{0.1}O_2$ cells with different electrolytes: (**a**) the cyclic performances at the charging/discharging rate of 0.2/0.5 C between 2.8 and 4.3 V vs. Li/Li^+; (**b**–**e**) the capacity–voltage curves; (**f**) the charging mid-voltage profiles; (**g**) the accumulated capacity of four electrolytes; (**h**) the rate performances.

The cyclic performance was evaluated under 0.2 C charge and 0.5 C discharge between 2.8 and 4.3 V vs. Li/Li^+, as shown in Figure 2a–e. The cells with the Base + FEC + LiBOB + ADN electrolytes present the highest capacity retention, retaining ~71.6% in the 250th cycle, which is significantly better than the samples of Base + FEC + LiBOB (129 cycles), the Base electrolytes (127 cycles) and the Base + ADN (80 cycles). Furthermore, the charging mid-capacity voltage of the cells with the Base + ADN electrolytes is the largest and increases faster than that of the other electrolytes, while the variation in the mid-capacity voltage with FEC and LiBOB is more stable than the Base (Figure 2f). The accumulated capacity of $Li/LiNi_{0.8}Co_{0.1}Mn_{0.1}O_2$ cells with Base + FEC + LiBOB + ADN electrolytes achieved a cumulative discharge capacity of ~653.36 mAh cm^{-2} with capacity retention ≈ 80%, while those of the Base, Base + ADN and Base + FEC + LiBOB electrolytes are 347.9, 194.6 and 360.0 mAh cm^{-2} (Figure 2g). These results demonstrate the usage of the ADN additive can boost the LIB's electrochemical performance when appropriate anodic protective strategies are used; however, it seriously deteriorates the cells' durability if no remedies are applied.

The electrochemical impedance spectra (EIS) of the $Li/LiNi_{0.8}Co_{0.1}Mn_{0.1}O_2$ full cells were assessed to evaluate the resistance of the Li^+ ion transport processes. As shown in Figure S2, the high-frequency and mid-frequency semicircles are related to the resistances of the electrode/electrolyte interphase (R_I) and the charge transfer on the surface of the electrode (R_{ct}), respectively. After 10 cycles, the R_I in the Base + ADN electrolytes is almost twice that in the FEC- and LiBOB-added electrolytes and constantly decreased over 20 cycles; meanwhile, that in the FEC- and LiBOB-added electrolytes was much more stable with cycling (Table S3). The R_{ct} in the Base electrolytes shows a large elevation over 20 cycles; meanwhile, that in the FEC- and LiBOB-added electrolytes displays a slight decrease. These results indicate that the FEC and LiBOB additives can construct a stable and low-resistance interfacial film and promote charge transfer on the surface.

To analyze the working mechanism of these electrolytes, the batteries that ran for 10 cycles and those that lost efficacy in the cycling process were disassembled. The morphologies and elemental components of the electrode surfaces were observed with a scanning electron microscope (SEM) and energy-dispersive spectroscopy (EDS). As shown in Figures 3a–h and S5, compared to the fresh Li metal, the surface morphologies of the Li anode that was cycled for 10 cycles in the Base and Base + ADN electrolytes are loose and porous, and a significant quantity of coarse sediment can be observed on the anode cycled in the Base + ADN electrolytes. In contrast, the surfaces of the Li anode are significantly denser and smoother following cycling in the electrolytes with the FEC and LiBOB additives, whether ADN was added or not. As shown in Figure S6, the Li metal anodes of the Base (127 cycles) and the Base + ADN (80 cycles) electrolytes that lost their efficacy both produced thick and loose deposits, and the addition of ADN significantly increased the Li metal consumption. In sharp contrast, the Base + FEC + LiBOB electrolytes retained a partial Li metal anode morphology even after 129 cycles of loss of efficacy, despite the reaction producing a rough material. A similar situation occurred with the batteries using the Base + FEC + LiBOB + ADN electrolytes after more than 250 cycles. As shown in Table S4, some transitional metals of Ni, Co and Mn with an atomic ratio of ~10% were observed on the anode side in the cells with the electrolytes of Base, Base + ADN and Base + FEC + LiBOB, indicating the electrolyte corrosion took place in these systems. In sharp contrast, the total amount of transition metal was reduced to less than 1.4% when the cells used the electrolytes with FEC + LiBOB + ADN. These results indicate that ADN protects the cathode particles via an absorbing CEI layer and SEI layer formed from FEC and LiBOB, which alleviates the decomposition of the ADN additive.

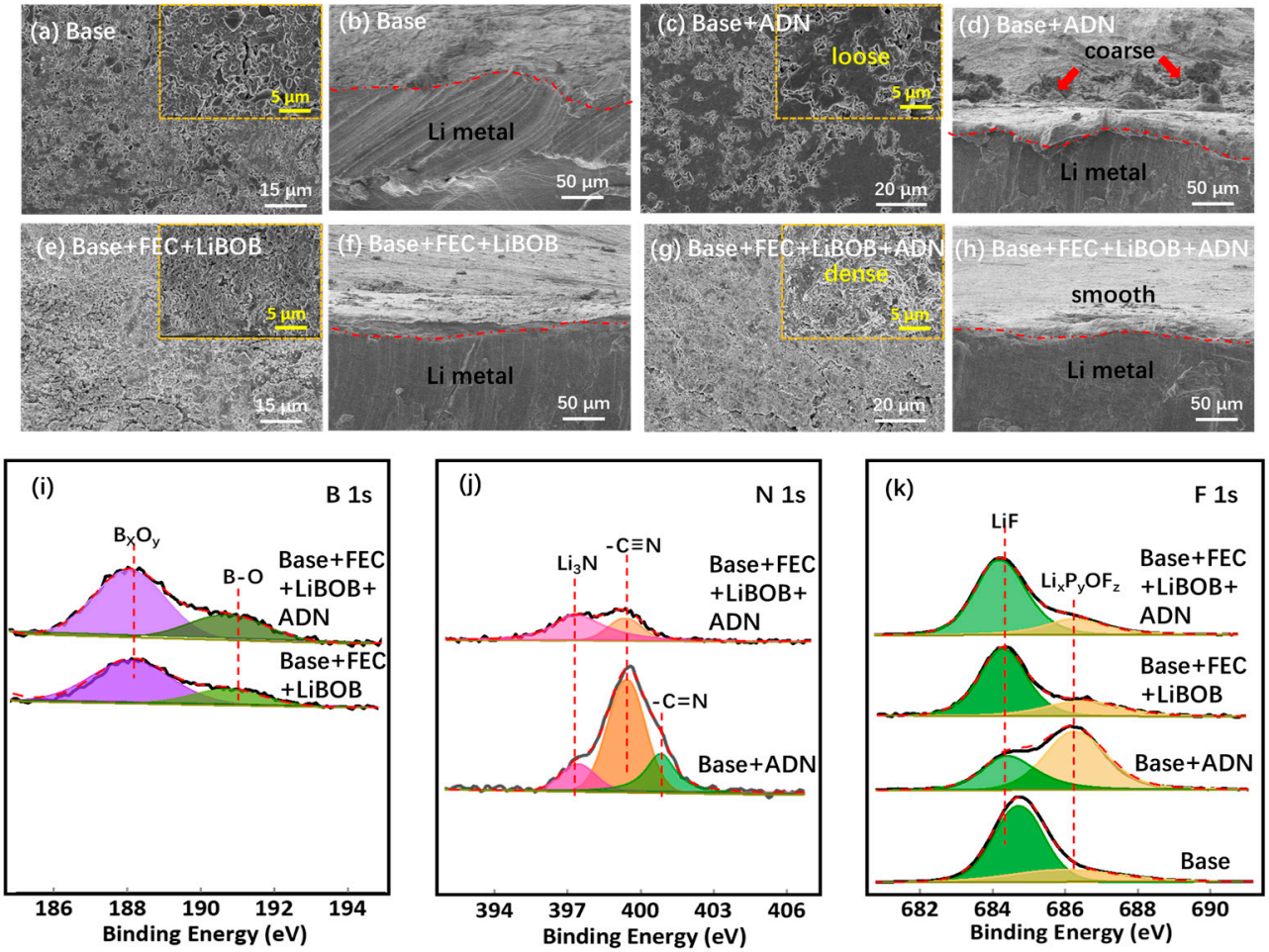

Figure 3. (**a**–**h**) SEM images of the cycled Li anode in Li/$LiNi_{0.8}Co_{0.1}Mn_{0.1}O_2$ cells after 10 cycles with four electrolytes: (**a**,**c**,**e**,**g**) the surface; (**b**,**d**,**f**,**h**) the cross-section; (**i**–**k**) the XPS spectra of the cycled Li anode; (**i**) B1s; (**j**) N1s; (**k**) F1s.

The chemical components on the cycled Li anode were detected via X-ray photoelectron spectroscopy (XPS) measurements. As shown in Figure 3i, there are two peaks pointing to boron and borate compounds at 188.3 and 191.0 eV in the B 1s spectra [18,19], which are probably derived from the LiBOB additive of the Base + FEC + LiBOB and Base + FEC + LiBOB + ADN electrolytes. In the N 1s spectra (Figure 3j), three peaks corresponding to Li_3N, -CN and -C=N compounds at 398.2 [20], 400.1 [14] and 401.4 eV [21] can be clearly seen with the Base + ADN electrolyte, which should be generated from the decomposition of the ADN additive. However, with the multiple additives of FEC, LiBOB and ADN, the intensities of the -CN and Li_3N peaks are much weaker. In the F 1s spectra (Figure 3k), two peaks relating to LiF and $Li_xP_yOF_z$ at 684.6 and 686.6 eV can be seen in four electrolytes [22,23], but the ratio of LiF is less in the Base + ADN electrolytes than the other electrolytes. These results further indicate that the FEC and LiBOB additives can be decomposed to form an F- and B-enriched passivation layer, suppressing the decomposition of the ADN additive on the anode. In addition, in the C 1s and O 1s spectra (Figures S7 and S8), the inorganic Li_2O and boron compound peaks can be seen in the electrolytes with FEC and LiBOB added; meanwhile, the -CN peak can be detected in the Base + ADN electrolyte. In the P 2p spectra (Figure S9), the intensities of the $Li_xP_yOF_z$ and Li_xPF_y peaks are much weaker in the FEC- and LiBOB-added electrolytes than in the Base + ADN electrolytes. These demonstrate that the passivation layers that evolved from the FEC and LiBOB suppress the decomposition of the PF_6^- anions.

A scanning electron microscope (SEM) and a transmission electron microscope (TEM) were used for the observation of the cycled Li anode in the Li/$LiNi_{0.8}Co_{0.1}Mn_{0.1}O_2$ cells after 10 cycles and identified a loss in efficacy. As shown in Figures 4 and S9, coarse deposits can be observed on the surfaces of the cathode particles after 10 cycles in the Base and Base + FEC + LiBOB electrolytes compared to the original electrodes. In the electrolytes with ADN added, the surface is smoother. The formed thin CEI films are faintly visible in the Base + ADN, Base + FEC + LiBOB and Base + FEC + LiBOB + ADN electrolytes. This continues until the cells lose efficacy. In Figure S11, the surfaces of the cathode material of the Base and Base + FEC + LiBOB are bound by rough material. In contrast, the cathode particles of the electrolytes with ADN added are smooth, which is the same as when cycled for 10 cycles. The cathode particles of these four electrolytes assume a different state after cycling to the end of their life. The $LiNi_{0.8}Co_{0.1}Mn_{0.1}O_2$ electrode particles of the Base electrolytes (127 cycles) and the Base + ADN electrolytes (80 cycles) are obviously stratified. The cathode particle consumption of the Base + FEC + LiBOB electrolytes (128 cycles) is severe; after more than 250 cycles, no stratification is observed in the Base + FEC + LiBOB + ADN electrolytes. These results indicate the combination of multiple additives can form a stable CEI film on the cathode.

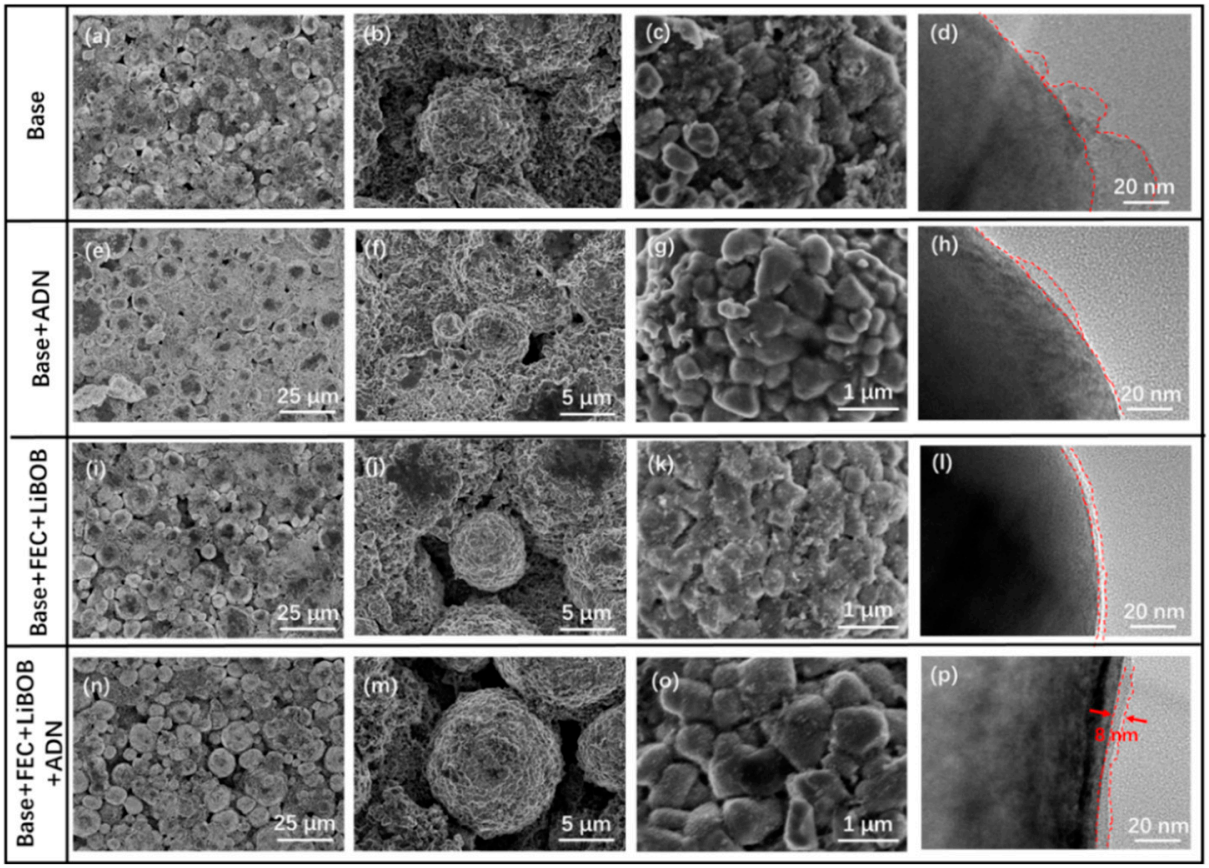

Figure 4. The SEM and TEM images of the 10 cycled $LiNi_{0.8}Co_{0.1}Mn_{0.1}O_2$ electrodes in four electrolytes: (**a**–**d**) Base electrolyte; (**e**–**h**) Base + ADN electrolyte; (**i**–**l**) Base + FEC + LiBOB electrolyte; (**m**–**p**) Base + FEC + LiBOB + ADN electrolyte; (**d**,**h**,**l**,**p**) the morphologies obtained using TEM.

The structures of the $LiNi_{0.8}Co_{0.1}Mn_{0.1}O_2$ electrodes before and after 10 cycles were measured using X-ray diffraction (XRD) equipment. As shown in Figure 5a, the feature peaks of the (003), (101) and (104) layered oxide materials are clearly visible for the fresh and cycled electrodes. The (003) peaks of the cathodes cycled in electrolytes without ADN are slightly shifted to 18.4° from 18.6°; meanwhile, no change takes place in the electrodes cycled in ADN-containing electrolytes. The surficial components of the cycled

$LiNi_{0.8}Co_{0.1}Mn_{0.1}O_2$ particles were detected with XPS. As shown in Figure 5b–d, the peaks of the -CN group located at 287.1 and 399.3 eV in the C1s and N1s spectra are observed in the Base + FEC + LiBOB + ADN electrolytes. In addition, the area ratio of the LiF in the F1s spectra is much higher than that in the Base and Base + ADN electrolytes and is slightly higher than that in the Base + FEC + LiBOB electrolytes. Due to their good stability at a high voltage, both the LiF and -CN groups are considered to be important components of CEI film for suppressing interfacial reactions. Moreover, in the O 1s and P 2p spectra, strong peaks of $Li_xP_yOF_z$ in the Base and the Base + ADN electrolytes are detectable, implying the serious decomposition of the PF_6^- anions (Figure S12 and S13). There are weak peaks of B-containing compounds and strong peaks of Ni to be seen in the Base + FEC + LiBOB and Base + FEC + LiBOB + ADN electrolytes (Figures S13 and S14). These results indicate the ADN could effectively protect the cathode and suppress the decomposition of electrolytes when FEC and LiBOB are co-utilized together.

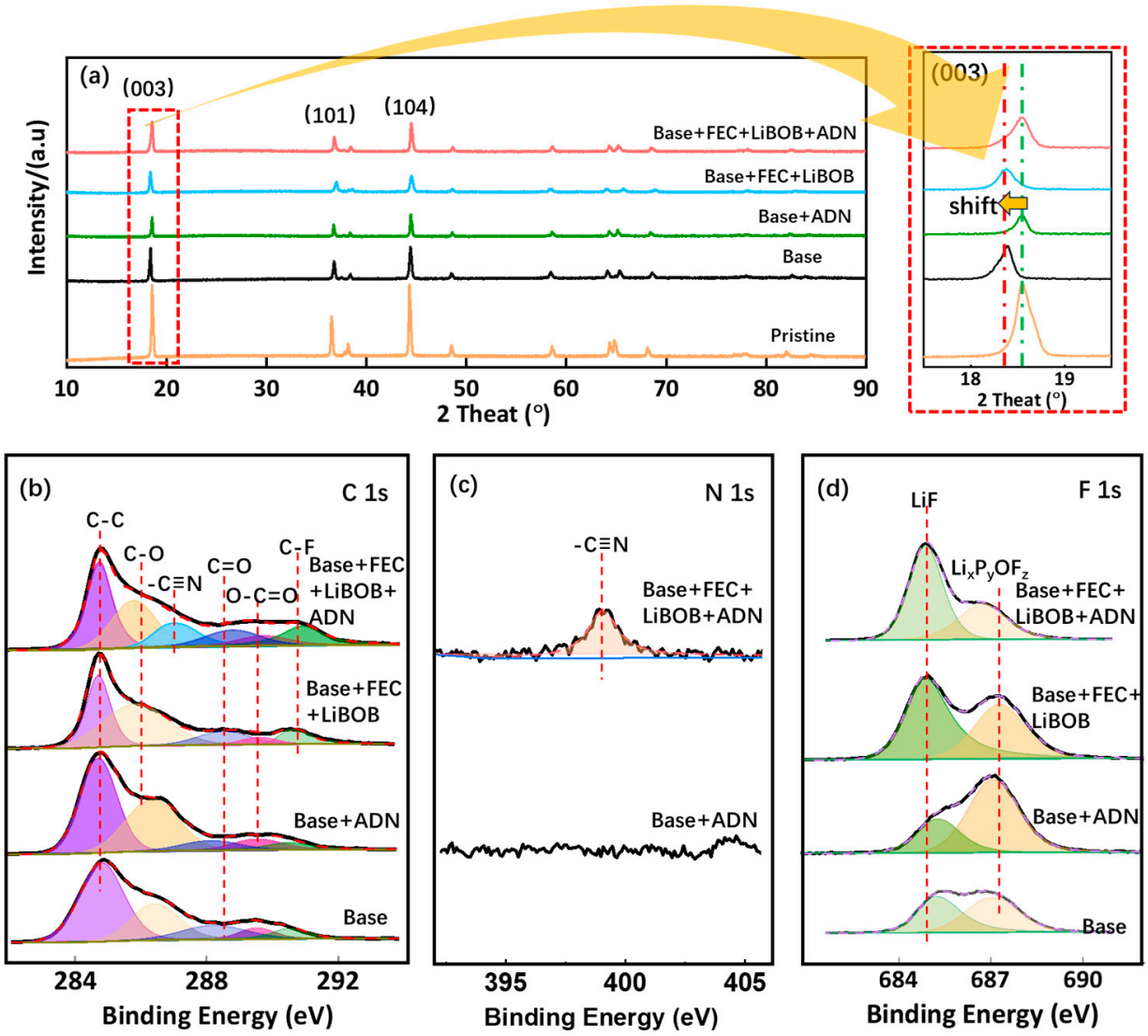

Figure 5. (**a**) XRD spectra of $LiNi_{0.8}Co_{0.1}Mn_{0.1}O_2$ electrodes cycled in four electrolytes; (**b**–**d**) XPS spectra of cycled $LiNi_{0.8}Co_{0.1}Mn_{0.1}O_2$ electrodes: (**b**) C 1s; (**c**) N 1s; (**d**) F 1s.

3. Conclusions

In this study, the additives of FEC, LiBOB and ADN were adopted to synchronously construct an in situ SEI film on a Li metal anode and a stable CEI film on a Ni-rich cathode. The B-containing and LiF-enriched SEI film formed from FEC and LiBOB was identified as

being able to suppress the decomposition of ADN on Li metal. Thereby, ADN can fully exert its positive effects to protect the cathode particles from the high-ratio F-containing solvents. Under the protection of the films formed synchronously on both electrodes, the Li-$LiNi_{0.8}Co_{0.1}Mn_{0.1}O_2$ cells with an area capacity of ~3 mAh cm^{-2} show a stable cycle performance beyond 250 cycles with a capacity retention of ~71.7% and an average Coulombic efficiency of 99.77%. Our approach demonstrates that appropriate electrolyte engineering plays a crucial role in the development of lithium metal batteries.

4. Experimental Section

The materials for preparing the electrolytes, including EC, DEC, FEC, ADN, $LiPF_6$ and LiBOB salts, were purchased commercially from Langu New Energy Co., Ltd., Liyang, China. All the electrolytes were prepared in an argon-filled glovebox (H_2O and O_2 contents < 1 ppm). The base electrolyte consisted of 2 M $LiPF_6$ dissolved in mixed solvents of EC and DEC (1:1, *v*/*v*). Base + ADN, Base + FEC + LiBOB and Base + FEC + LiBOB + ADN electrolytes were composed of Base electrolytes with 1.0 wt.% ADN, 30.8 wt.% FEC, 1.2 wt.% LiBOB, 30.8 and 1.2 wt.% FEC and LiBOB and 30.8 and 1.2 and 1.0 wt.% FEC and LiBOB and ADN added, respectively. The Super-P electrodes were composed of Super-P and PVDF (8:2, *w*/*w*), which were separately coated on both Cu and Al foil current collectors for low-potential and high-potential tests. The $LiNi_{0.8}Co_{0.1}Mn_{0.1}O_2$ electrodes comprised active materials, Super-P and PVDF (98:1:1, *w*/*w*).

The cyclic performance of the Li/$LiNi_{0.8}Co_{0.1}Mn_{0.1}O_2$ and Li/Li symmetric cells was assessed with Land CT2001A multi-channel battery cycler equipment. The Li/$LiNi_{0.8}Co_{0.1}Mn_{0.1}O_2$ cells were activated at a charging/discharging rate of 0.1/0.1 C for 3 cycles. The CV and LSV of the Li/Super-P cells were determined with a Solartron electrochemical workstation with a scan rate of 0.1 mV s^{-1}. The electrochemical impedance of the Li/$LiNi_{0.8}Co_{0.1}Mn_{0.1}O_2$ cells was also determined with a Solartron workstation with an amplitude of 10 mV, a scan rate of 0.1 mV/S and a frequency range of 0.1–10^{-5} Hz. The amount of electrolyte added was 70 μL per cell.

The ionic conductivity testing of the electrolytes was performed in an argon-filled glovebox (H_2O and O_2 contents < 1 ppm) using an INESA DDS-307A Ionic Conductivity Meter at an ambient temperature of ~25 °C.

The surface morphologies of the Li anode and the $LiNi_{0.8}Co_{0.1}Mn_{0.1}O_2$ cathode were observed using SEM (FESEM, Regulus-8230; Hitachi, Tokyo, Japan) and TEM (JEM-2100; Nidec Corporation, Tokyo, Japan). The chemical compositions of the Li and $LiNi_{0.8}Co_{0.1}Mn_{0.1}O_2$ electrode surfaces were analyzed using XPS (AXIS ULTRA; Kratos Analytica, Manchester, UK) with a monochromated Al Kα line as an X-ray source. The crystal structure of the $LiNi_{0.8}Co_{0.1}Mn_{0.1}O_2$ electrode was tested with XRD (Empyrean; PANalytical B.V., The Netherlands) with a Cu Kα radiation source, using a mixed Gaussian–Lorentzian fit.

Supplementary Materials: The following supporting information can be downloaded at: https://www.mdpi.com/article/10.3390/batteries10100338/s1. Table S1. Ionic conductivities of four electrolytes at 25 °C; Table S2. the electrochemical performance of Li/$LiNi_{0.8}Co_{0.1}Mn_{0.1}O_2$ cells in 1st cycle; Table S3. The EIS analysis of Li/$LiNi_{0.8}Co_{0.1}Mn_{0.1}O_2$ cells; Table S4. Element ratio of cycled Li anode in different electrolytes by EDS measurement; Figure S1. The capacity-voltage profiles of Li/LiNi0.8Co0.1Mn0.1O2 cells in the first cycle with different electrolytes at the charging/discharging rate of 0.1/0.1 C between 2.8 and 4.3 V vs. Li/Li^+; Figure S2. CV profiles of Super-P/Li cells with (a,b) Base + FEC electrolyte, (c,d) Base + LiBOB electrolyte, (a,c) the first cycle, (b,d) the second cycle. Base + FEC and Base + LiBOB electrolytes correspond to Base electrolyte adding with FEC and LiBOB respectively and their contents refer to Base + FEC + LiBOB electrolyte; Figure S3. EIS of Li/LiNi0.8Co0.1Mn0.1O2 cells after being cycled in different electrolytes for (a) 10 cycles and (b) 20 cycles (the dot is the experimental data, the dot with line is the simulative data); Figure S4. The capacity-voltage profiles of Li/$LiNi_{0.8}Co_{0.1}Mn_{0.1}O_2$ cells at different charging/discharging rate (a) 0.1 C (b) 0.2 C (c) 1 C (d) 2 C; Figure S5. The surface and cross-sectional morphologies of fresh Li metal; Figure S6. SEM images of Li-anode cross-sectional morphologies circulating to lose efficacy

in four electrolytes; Figure S7. C1s spectra of cycled Li anode by XPS (a) Base electrolyte, (b) Base + ADN electrolyte, (c) Base + FEC + LiBOB electrolyte, (d) Base + FEC + LiBOB + ADN electrolyte; Figure S8. O 1s spectra of cycled Li anode by XPS (a) Base electrolyte, (b) Base + ADN electrolyte, (c) Base + FEC + LiBOB electrolyte, (d) Base + FEC + LiBOB + ADN electrolyte; Figure S9. P 2p spectra of cycled Li anode by XPS (a) Base electrolyte, (b) Base + ADN electrolyte, (c) Base + FEC + LiBOB electrolyte, (d) Base + FEC + LiBOB + ADN electrolyte; Figure S10. The morphology images of pristine LiNi0.8Co0.1Mn0.1O2 electrode by (a–c) SEM (d) TEM; Figure S11. SEM images of LiNi0.8Co0.1Mn0.1O2 electrodes after cycling in four electrolytes, (a,b) Base electrolyte (127cycle), (c,d) Base + ADN electrolyte (88 cycle), (e,f) Base + FEC + LiBOB electrolyte (128 cycle), (g,h) Base + FEC + LiBOB + ADN electrolytes (250 cycle); Figure S12. O 1s spectra of cycled LiNi0.8Co0.1Mn0.1O2 electrodes by XPS (a) Base electrolyte, (b) Base + ADN electrolyte, (c) Base + FEC + LiBOB electrolyte, (d) Base + FEC + LiBOB + ADN electrolyte; Figure S13. P 2p spectra of cycled LiNi0.8Co0.1Mn0.1O2 electrodes by XPS (a) Base electrolyte, (b) Base + ADN electrolyte, (c) Base + FEC + LiBOB electrolyte, (d) Base + FEC + LiBOB + ADN electrolyte; Figure S14. B 1s spectra of cycled $LiNi_{0.8}Co_{0.1}Mn_{0.1}O_2$ electrodes by XPS (a) Base + FEC + LiBOB electrolyte, (b) Base + FEC + LiBOB + ADN electrolyte; Figure S15. Ni 2p spectra of cycled $LiNi_{0.8}Co_{0.1}Mn_{0.1}O_2$ electrodes by XPS (a) Base electrolyte, (b) Base + ADN electrolyte, (c) Base + FEC + LiBOB electrolyte, (d) Base + FEC + LiBOB + ADN electrolyte.

Author Contributions: Conceptualization, D.W., Y.Q. and Y.W.; methodology, Y.W.; software, S.C., Z.C.; validation, Y.Q., Y.W., C.S. and W.B.; formal analysis, Y.W.; investigation, Y.W. and S.W.; resources, D.W. and M.W. (Muqin Wang). and M.W. (Mingkui Wang); data curation, Y.W. and W.B.; writing—original draft preparation, Y.Q. and Y.W.; writing—review and editing, Y.Q., D.W. and Y.W.; visualization, Y.Q. and Y.W.; supervision, D.W. and Z.C.; project administration, D.W. and M.W. (Muqin Wang); funding acquisition, D.W. and M.W. (Muqin Wang). All authors have read and agreed to the published version of the manuscript.

Funding: This research was funded by the National Natural Science Foundation of China (22179052), National Natural Science Foundation of China Youth (22209052) and the Excellent Discipline Cultivation Project funded by Jianghan University (2023XKZ013).

Data Availability Statement: The original contributions presented in the study are included in the article, further inquiries can be directed to the corresponding author.

Conflicts of Interest: The authors declare no conflicts of interest.

References

1. Tan, S.J.; Wang, W.P.; Tian, Y.F.; Xin, S.; Guo, Y.G. Advanced Electrolytes Enabling Safe and Stable Rechargeable Li-Metal Batteries: Progress and Prospects. *Adv. Funct. Mater.* **2021**, *31*, 2105253. [CrossRef]
2. Yuan, S.; Kong, T.; Zhang, Y.; Dong, P.; Zhang, Y.; Dong, X.; Wang, Y.; Xia, Y. Advanced Electrolyte Design for High-Energy-Density Li-Metal Batteries under Practical Conditions. *Angew. Chem. Int. Ed.* **2021**, *60*, 25624–25638. [CrossRef] [PubMed]
3. Wu, F.; Fang, S.; Kuenzel, M.; Mullaliu, A.; Kim, J.-K.; Gao, X.; Diemant, T.; Kim, G.-T.; Passerini, S. Dual-anion ionic liquid electrolyte enables stable Ni-rich cathodes in lithium-metal batteries. *Joule* **2021**, *5*, 2177–2194. [CrossRef]
4. Wang, X.; Bai, Y.; Wang, X.; Wu, C. High-Voltage Layered Ternary Oxide Cathode Materials: Failure Mechanisms and Modification Methods. *Chin. J. Chem.* **2020**, *38*, 1847–1869. [CrossRef]
5. Horstmann, B.; Shi, J.; Amine, R.; Werres, M.; He, X.; Jia, H.; Hausen, F.; Cekic-Laskovic, I.; Wiemers-Meyer, S.; Lopez, J.; et al. Strategies towards enabling lithium metal in batteries: Interphases and electrodes. *Energy Environ. Sci.* **2021**, *14*, 5289–5314. [CrossRef]
6. Qin, D.; Cheng, F.; Zhang, W.; Xu, J.; Sun, S.; Xu, Y.; Fang, C.; Han, J. Electrolyte regulating and interface engineering for high voltage $LiCoO_2$ lithium metal batteries. *Appl. Surf. Sci.* **2023**, *616*, 156447. [CrossRef]
7. Guo, Y.; Li, H.; Zhai, T. Reviving Lithium-Metal Anodes for Next-Generation High-Energy Batteries. *Adv. Mater.* **2017**, *29*, 1700007. [CrossRef]
8. Yang, X.; Wang, C.; Yan, P.; Jiao, T.; Hao, J.; Jiang, Y.; Ren, F.; Zhang, W.; Zheng, J.; Cheng, Y.; et al. Pushing Lithium Cobalt Oxides to 4.7 V by Lattice-Matched Interfacial Engineering. *Adv. Energy Mater.* **2022**, *12*, 2200197. [CrossRef]
9. Tan, S.; Shadike, Z.; Li, J.; Wang, X.; Yang, Y.; Lin, R.; Cresce, A.; Hu, J.; Hunt, A.; Waluyo, I.; et al. Additive engineering for robust interphases to stabilize high-Ni layered structures at ultra-high voltage of 4.8 V. *Nat. Energy* **2022**, *7*, 484–494. [CrossRef]
10. Qin, Y.; Xu, K.; Wang, Q.; Ge, M.; Cheng, T.; Liu, M.; Cheng, H.; Hu, Y.; Shen, C.; Wang, D.; et al. In-situ constructing a rigid and stable dual-layer CEI film improving high-voltage 4.6 V $LiCoO_2$ performances. *Nano Energy* **2022**, *96*, 107082. [CrossRef]
11. Xue, W.; Gao, R.; Shi, Z.; Xiao, X.; Zhang, W.; Zhang, Y.; Zhu, Y.G.; Waluyo, I.; Li, Y.; Hill, M.R.; et al. Stabilizing electrode–electrolyte interfaces to realize high-voltage Li||$LiCoO_2$ batteries by a sulfonamide-based electrolyte. *Energy Environ. Sci.* **2021**, *14*, 6030–6040. [CrossRef]

12. Qiu, Y.; Lu, D.; Gai, Y.; Cai, Y. Adiponitrile (ADN): A Stabilizer for the $LiNi_{0.8}Co_{0.1}Mn_{0.1}O_2$ (NCM811) Electrode/Electrolyte Interface of a Graphite/NCM811 Li-Ion Cell. *ACS Appl. Mater. Interfaces* **2022**, *14*, 11398–11407. [CrossRef] [PubMed]
13. Kim, Y.-S.; Lee, H.; Song, H.-K. Surface Complex Formation between Aliphatic Nitrile Molecules and Transition Metal Atoms for Thermally Stable Lithium-Ion Batteries. *ACS Appl. Mater. Interfaces* **2014**, *6*, 8913–8920. [CrossRef] [PubMed]
14. Wang, X.; Zheng, X.; Liao, Y.; Huang, Q.; Xing, L.; Xu, M.; Li, W. Maintaining structural integrity of 4.5 V lithium cobalt oxide cathode with fumaronitrile as a novel electrolyte additive. *J. Power Sources* **2017**, *338*, 108–116. [CrossRef]
15. She, S.-X.; Zhou, Y.-L.; Hong, Z.; Huang, Y.; Wu, Y. Effect of FEC electrolyte additive on the electrochemical performance of nickel-rich NCM ternary cathode. 2023; unpublished work.
16. Qin, Y.; Wang, D.; Liu, M.; Shen, C.; Hu, Y.; Liu, Y.; Guo, B. Improving the Durability of Lithium-Metal Anode via In situ Constructed Multilayer SEI. *ACS Appl. Mater. Interfaces* **2021**, *13*, 49445–49452. [CrossRef]
17. Qin, Y.; Cheng, H.; Zhou, J.; Liu, M.; Ding, X.; Li, Y.; Huang, Y.; Chen, Z.; Shen, C.; Wang, D.; et al. A tough Janus-faced CEI film for high voltage layered oxide cathodes beyond 4.6 V. *Energy Storage Mater.* **2023**, *57*, 411–420. [CrossRef]
18. Li, S.; Liang, Y.; Xie, J.; Ai, L.; Xie, Y.; Li, C.; Wang, C.; Cui, X. Compatibility between lithium difluoro (oxalate) borate-based electrolytes and $Li_{1.2}Mn_{0.54}Ni_{0.13}Co_{0.13}O_2$ cathode for lithium-ion batteries. *J. Electroanal. Chem.* **2018**, *823*, 688–696. [CrossRef]
19. Liu, Y.; Wang, M.; Chen, J.; Yang, J.; Wang, K.; Ren, Z.; Xi, W.; Huang, Y.; Zheng, J.; Li, X. Performance enhanced high-nickel lithium metal batteries through stable cathode and anode electrolyte interfaces. *Sustain. Energy Fuels* **2020**, *4*, 2875–2883. [CrossRef]
20. Wang, Z.; Sun, Y.; Mao, Y.; Zhang, F.; Zheng, L.; Fu, D.; Shen, Y.; Hu, J.; Dong, H.; Xu, J.; et al. Highly concentrated dual-anion electrolyte for non-flammable high-voltage Li-metal batteries. *Energy Storage Mater.* **2020**, *30*, 228–237. [CrossRef]
21. Lee, S.H.; Hwang, J.Y.; Park, S.J.; Park, G.T.; Sun, Y.K. Adiponitrile ($C_6H_8N_2$): A New Bi-Functional Additive for High-Performance Li-Metal Batteries. *Adv. Funct. Mater.* **2019**, *29*, 1902496. [CrossRef]
22. Wu, D.; He, J.; Liu, J.; Wu, M.; Qi, S.; Wang, H.; Huang, J.; Li, F.; Tang, D.; Ma, J. Li_2CO_3/LiF-Rich Heterostructured Solid Electrolyte Interphase with Superior Lithiophilic and Li+-Transferred Characteristics via Adjusting Electrolyte Additives. *Adv. Energy Mater.* **2022**, *12*, 2200337. [CrossRef]
23. Su, H.; Chen, Z.; Li, M.; Bai, P.; Li, Y.; Ji, X.; Liu, Z.; Sun, J.; Ding, J.; Yang, M.; et al. Achieving Practical High-Energy-Density Lithium-Metal Batteries by a Dual-Anion Regulated Electrolyte. *Adv. Mater.* **2023**, *35*, 2301171. [CrossRef] [PubMed]